

Synthesis, structure, DNA and protein binding studies, and cytotoxic activity of nickel(II) complexes containing 3,3-dialkyl/aryl-1-(2,4-dichlorobenzoyl)thiourea ligands



N. Selvakumaran^a, N.S.P. Bhuvanesh^b, A. Endo^c, R. Karvembu^{a,*}

^a Department of Chemistry, National Institute of Technology, Tiruchirappalli 620015, India

^b Department of Chemistry, Texas A & M University, College Station, TX 77842, USA

^c Department of Materials and Life Sciences, Sophia University, 7-1 Kioicho, Chiyoda-ku, Tokyo 102-8554, Japan

ARTICLE INFO

Article history:

Received 3 January 2014

Accepted 10 March 2014

Available online 20 March 2014

Keywords:

Acylthiourea

Ni(II) complex

DNA binding

BSA interaction

Cytotoxicity

ABSTRACT

A new series of nickel(II) complexes of the type $[\text{Ni}(\text{L})_2]$ (**1–6**) has been synthesized by using the 3,3-dialkyl/aryl-1-(2,4-dichlorobenzoyl)thiourea ligands, and characterized by analytical and spectral (NMR, FT-IR and UV-Vis) techniques. The structures of the ligands (HL1, HL2 and HL3) and complexes (**2** and **5**) have been confirmed by single crystal X-ray diffraction studies. The interaction of the nickel(II) complexes (**2–5**) with calf thymus (CT) DNA and bovine serum albumin (BSA) protein was investigated using UV-Vis and fluorescence spectroscopic methods. Absorption and emission spectral studies indicate that complex **2** interacts with CT DNA and BSA protein more strongly than the other complexes (**3**, **4** and **5**). Complexes **2** and **5** exhibited good cytotoxicity against A549 and HT29 cell lines at 50 μM concentration.

© 2014 Elsevier Ltd. All rights reserved.

1. Introduction

Recently, several highly potent platinum metal-based drugs are used in the cancer treatment, with cisplatin, carboplatin, and oxaliplatin being widely used worldwide. However, several side effects and frequent development of resistance phenomena complicate and hamper the clinical applications [1,2]. A very promising strategy to overcome these obstacles is the use of specific carriers and the change from platinum to other transition metals [3–5]. The transition metal complexes play an important role in nucleic acids chemistry for their diverse applications such as foot printing agents, sequence specific binding, structural probes, and therapeutic agents [6–10]. Nickel is one of the most essential elements for biological systems and is present in the trace quantities [11]. The biological activity of the nickel has been rapidly expanded due to the increasing interest in nickel complexes, which have been shown to act as antiepileptic, anticonvulsant agents or vitamins or have shown antibacterial, antifungal, antimicrobial and anticancer/antiproliferative activities [12–19]. Several reports described the reactivity of DNA with mononuclear nickel(II) complexes [20–23]. Nickel(II) complexes with 2-phenylquinoline-4-carboxylic acid hydrazide ligand showed significant cytotoxicity

against MFC cell lines and also bind DNA via a groove binding mode; further, these complexes can cleave pBR322 DNA [24]. Nickel(II) complexes of benzoic acid(2-hydroxy-benzylidene)hydrazide ligands bind to DNA base pairs via intercalation and π - π stacking interactions; *in vitro* free radical scavenging and cytotoxic potential have also been investigated [25]. Nickel(II) complexes containing N-substituted heterocyclic thiosemicarbazones were found to exhibit excellent DNA/protein binding and antioxidant properties; the binding ability of these complexes varies with the N-terminal substituents [26].

DNA binding ability and cytotoxic activity of thiourea complexes have also been investigated. A new class of hybrid platinum compounds containing acridinylthiourea as intercalating group and its analogs exhibit promising activity toward several tumor cell lines, and show only partial cross resistance with cisplatin [27–29]. Acylthiourea ligands are of considerable interest to inorganic chemists because of their variable coordination behavior and promising biological activities [30–38].

A survey of the literature revealed that there is no benzoyl thiourea ligand reported with two chloro substituents in the benzoyl moiety. Binzet et al. reported the synthesis and characterization of copper(II) and nickel(II) complexes of some 4-bromo-N-(di(alkyl/aryl)carbamothioyl)benzamide derivatives [39]. Arslan et al. prepared copper(II), nickel(II) and cobalt(II) complexes of 4-chloro-N-(di(alkyl/aryl)carbamothioyl)benzamide, and copper(II) and zinc(II)

* Corresponding author. Tel.: +91 431 2503631; fax: +91 431 2500133.

E-mail address: kar@nitt.edu (R. Karvembu).

complexes with N-pyrrolidine-N'-(2-chlorobenzoyl)thiourea derivatives [40]. Chelating difluoro-substituted acylthiourea ligands were also reported [41]. In our previous reports, we have disclosed the synthesis and cytotoxicity of palladium(II) and nickel(II) complexes containing 3,3-dialkyl/aryl-1-benzoylthiourea ligands [42,43]. We report here the synthesis and characterization of six 3,3-diaryl/alkyl-1-(2,4-dichlorobenzoyl)thiourea ligands and their nickel(II) complexes. We have also established the potential of these complexes in DNA and protein interactions, and cytotoxicity.

2. Experimental

2.1. Materials and methods

All the chemicals were purchased from Sigma Aldrich and used as received. A549 (human lung cancer cell line) and HT29 (human colon adenocarcinoma cell line) were purchased from NCCS, Pune for cell culture experiments. Solvents were purified according to the standard procedures. Elemental analysis was carried out on a Vario EL-III elemental analyzer. Fourier transform infrared (FT-IR) spectra were obtained on a Nicolet-iS5 spectrophotometer as KBr pellets. UV-Vis spectra were recorded using a Shimadzu-2600 spectrophotometer operating in the range of 200–900 nm. Emission spectra were measured on a Jasco V-630 spectrophotometer using 5% DMF in buffer as the solvent. NMR spectra were recorded in CDCl₃ by using TMS as an internal standard on a Bruker 400 MHz spectrometer.

2.2. Synthesis of the ligands

A solution of 2,4-dichlorobenzoyl chloride (2.0946 g, 10 mmol) in acetone (60 mL) was added drop wise to a suspension of potassium thiocyanate (0.9718 g, 10 mmol) in anhydrous acetone (60 mL). The reaction mixture was heated under reflux for 45 minutes and then cooled to room temperature. A solution of secondary amine (0.7314–1.9728 g, 10 mmol) in acetone (60 mL) was added and the resulting mixture was stirred for 2 h at 27 °C. Hydrochloric acid (0.1 N, 500 mL) was added and the resulting white solid was filtered off, washed with water and dried *in vacuo*. Single crystals for X-ray diffraction studies were grown at room temperature from acetonitrile solutions of the HL1, HL2 and HL3.

2.2.1. 3,3-Diethyl-1-(2,4-dichlorobenzoyl)thiourea (HL1)

Yield: 82%. White. m.p. 142 °C. *Anal. Calc.* for C₁₂H₁₄Cl₂N₂OS (%): C, 47.22; H, 4.62; N, 9.18; S, 10.51. Found: C, 47.19; H, 4.58; N, 9.15; S, 10.55%. FT-IR (KBr): ν , cm⁻¹ 1654 (C=O), 1222 (C-S), 3237 (N-H). ¹H NMR (400 MHz, CDCl₃): δ , ppm 8.45 (s, 1H), 7.61–7.32 (m, 3H), 3.98–3.64 (m, 4H), 1.32–1.31 (m, 6H). ¹³C NMR (100 MHz, CDCl₃): δ , ppm 177.9 (C-S), 162.2 (C=O), 138.1, 132.2, 132.1, 131.5, 130.4, 127.8 (C₆H₅), 47.8, 48.1 (CH₂), 13.4, 11.4 (CH₃).

2.2.2. 3,3-Diisobutyl-1-(2,4-dichlorobenzoyl)thiourea (HL2)

Yield: 68%. White. m.p. 153 °C. *Anal. Calc.* for C₁₆H₂₂Cl₂N₂OS (%): C, 61.54; H, 4.23; N, 6.52; S, 7.47. Found: C, 61.51; H, 4.19; N, 6.55; S, 7.45. FT-IR (KBr): ν , cm⁻¹ 1701 (C=O), 1210 (C-S), 3181 (N-H). ¹H NMR (400 MHz, CDCl₃): δ , ppm 8.65 (s, 1H), 7.62–7.60 (d, *J* = 8.4 Hz, 1H), 7.46–7.45 (d, *J* = 1.6 Hz, 1H), 7.36–7.33 (dd, *J* = 8.4 & 1.6 Hz, 1H), 2.36–2.29 (m, 4H), 2.16–2.09 (m, 2H), 1.02 (d, *J* = 6.4 Hz, 6H), 0.91–0.93 (d, *J* = 6.4 Hz, 6H). ¹³C NMR (100 MHz, CDCl₃): δ , ppm 179.1 (C-S), 161.3 (C=O), 137.9, 132.2, 132.0, 131.2, 130.3, 127.7 (C₆H₅), 61.7 (CH₂-N), 60.7 (CH₂-N), 27.8, 26.0 (CH), 20.1, 20.0 (CH₃).

2.2.3. 3,3-Dibenzyl-1-(2,4-dichlorobenzoyl)thiourea (HL3)

Yield: 76%. Greenish yellow. m.p. 168 °C. *Anal. Calc.* for C₂₂H₁₈Cl₂N₂OS (%): C, 53.18; H, 6.14; N, 7.75; S, 8.87. Found: C, 53.22; H, 6.10; N, 7.69; S, 8.92. FT-IR (KBr): ν , cm⁻¹ 1702 (C=O), 1243 (C-S), 3257 (N-H). ¹H NMR (400 MHz, CDCl₃): δ , ppm 8.70 (s, 1H), 7.57 (d, *J* = 6.8 Hz, 1H), 7.43 (t, *J* = 1.2 Hz, 1H), 7.36–7.38 (m, 10 H), 7.12 (s, 1H), 5.17 (s, 2H), 4.75 (s, 2H). ¹³C NMR (100 MHz, CDCl₃): δ , ppm 180.6 (C-S), 162.3 (C=O), 138.2, 132.2, 131.7, 131.6, 130.5, 129.1, 128.9, 128.4, 127.9, 127.8 (C₆H₅), 56.4, 55.9 (CH₂).

2.2.4. 3,3-Diphenyl-1-(2,4-dichlorobenzoyl)thiourea (HL4)

Yield: 72%. White. m.p. 161 °C. *Anal. Calc.* for C₂₀H₁₄Cl₂N₂OS (%): C, 59.86; H, 3.52; N, 6.98; S, 7.99. Found: C, 59.82; H, 3.55; N, 7.01; S, 7.95%. FT-IR (KBr): ν , cm⁻¹ 1693 (C=O), 1371 (C-S), 3374 (N-H). ¹H NMR (400 MHz, CDCl₃): δ , ppm 8.57 (s, 1H), 7.62 (t, *J* = 1.2 Hz, 1H), 7.51 (t, *J* = 1.2 Hz, 1H), 7.42–7.48 (m, 10 H), 7.21 (s, 1H). ¹³C NMR (100 MHz, CDCl₃): δ , ppm 180.6 (C-S), 162.3 (C=O), 138.2, 132.2, 131.7, 131.6, 130.5, 129.1, 128.9, 128.4, 127.9, 127.8 (C₆H₅).

2.2.5. 3,3-Di-*n*-butyl-1-(2,4-dichlorobenzoyl)thiourea (HL5)

Yield: 64%. White. m.p. 158 °C. *Anal. Calc.* for C₁₆H₂₂Cl₂N₂OS (%): C, 53.18; H, 6.14; N, 7.75; S, 8.87. Found: C, 53.15; H, 6.09; N, 7.78; S, 8.84%. FT-IR (KBr): ν , cm⁻¹ 1677 (C=O), 1202 (C-S), 3186 (N-H). ¹H NMR (400 MHz, CDCl₃): δ , ppm 8.56 (s, 1H), 7.60 (d, *J* = 6.4 Hz, 1H), 7.45 (s, 1H), 7.35–7.33 (dd, *J* = 7.6 & 1.2 Hz, 1H), 3.92 (s, 2H), 3.58 (t, *J* = 6.4 Hz, 2H), 1.76–1.66 (m, 4H), 1.44–1.28 (m, 4H), 0.99–0.91 (m, 6H). ¹³C NMR (100 MHz, CDCl₃): δ , ppm 178.3 (C-S), 161.9 (C=O), 137.9, 132.1, 132.0, 131.3, 130.3, 127.7 (C₆H₅), 53.2 (CH₂-N), 30.1, 28.3, 20.1, 20.6 (CH₂), 13.8, 13.7 (CH₃).

2.2.6. 3,3-Diisopropyl-1-(2,4-dichlorobenzoyl)thiourea (HL6)

Yield: 74%. Pale yellow. m.p. 152 °C. *Anal. Calc.* for C₁₄H₁₈Cl₂N₂OS (%): C, 50.45; H, 5.44; N, 8.41; S, 9.62. Found: C, 50.37; H, 5.40; N, 8.35; S, 9.21. FT-IR (KBr): ν , cm⁻¹ 1664 (C=O), 1213 (C-S), 3171 (N-H). ¹H NMR (100 MHz, CDCl₃): δ , ppm 8.35 (s, 1H), 7.62 (d, *J* = 8.4 Hz, 1H), 7.44 (d, *J* = 1.6 Hz, 1H), 7.33 (dd, *J* = 8.4 & 2.0 Hz, 1H), 3.42–3.31 (m, 2H), 1.71–1.29 (m, 12H). ¹³C NMR (100 MHz, CDCl₃): δ , ppm 172.8 (C-S), 161.8 (C=O), 137.7, 132.4, 132.0, 131.3, 130.3, 127.6 (C₆H₅), 48.2 (CH), 20.0, 19.3 (CH₃).

2.3. Synthesis of nickel(II) complexes

3,3-Dialkyl/aryl-1-(2,4-dichlorobenzoyl)thiourea (HL1–HL6) (0.6080–0.85651 g, 2 mmol) dissolved in ethanol (30 mL) was added to ethanol (30 mL) solution of NiCl₂·6H₂O (0.2377 g, 1 mmol). Then, NaOAc (0.1620 g, 4 mmol) dissolved in the minimum amount of water was added. The reaction mixture was stirred at 27 °C for 2 h; a solid product was formed. The product was isolated by filtration, washed with diethyl ether and dried *in vacuo*. Suitable crystals for X-ray diffraction studies were grown at room temperature from the dichloromethane solutions of **2** and **5**.

2.3.1. [Ni(LI)₂] (**1**)

Yield: 65%. Dark brown. m.p. 166 °C. *Anal. Calc.* for C₂₄H₂₆Cl₄NiN₄O₂S₂ (%): C, 43.21; H, 3.93; N, 8.40; S, 9.61. Found: C, 43.18; H, 3.95; N, 8.38; S, 9.58%. UV-Vis (5% DMF in buffer): λ_{max} , nm (ϵ , dm³ mol⁻¹ cm⁻¹) 247 (31250), 295 (43200), 371 (14924). FT-IR (KBr): ν , cm⁻¹ 1375 (C=O), 1205 (C-S). ¹H NMR (400 MHz, CDCl₃): δ , ppm 7.65–7.16 (m, 6H), 3.73–3.72 (m, 8H), 1.27–1.24 (t, *J* = 5.6 Hz, 6H), 1.16–1.13 (t, *J* = 5.6 Hz, 6H). ¹³C NMR (100 MHz, CDCl₃): δ , ppm 172.5 (C-S), 171.9 (C=O), 135.8, 135.2, 133.5, 132.3, 130.4, 126.5 (C₆H₅), 46.0, 45.5 (CH₂), 13.3, 12.4 (CH₃).

2.3.2. [Ni(L2)₂] (2)

Yield: 68%. Brown. m.p. 176 °C. *Anal. Calc.* for C₃₂H₄₂Cl₄NiN₄O₂S₂ (%): C, 49.32; H, 5.43; N, 7.19; S, 8.23. Found: C, 49.35; H, 5.41; N, 7.16; S, 8.25%. UV–Vis (5% DMF in buffer): λ_{max}, nm (ε, dm³ mol⁻¹ cm⁻¹) 243 (32000), 299 (48400), 382 (14796). FT–IR (KBr): ν, cm⁻¹ 1415 (C–O), 1211 (C–S). ¹H NMR (400 MHz, CDCl₃): δ, ppm 7.66 (d, *J* = 8.4, 2H), 7.34 (d, *J* = 1.6 Hz, 2H), 7.19–7.17 (dd, *J* = 8.4 & 1.6 Hz, 2H), 3.56 (t, *J* = 7.2 Hz, 8H), 2.38–2.29 (m, 2H), 2.28–2.09 (m, 2H), 0.94–0.85 (m, 6H). ¹³C NMR (100 MHz, CDCl₃): δ, ppm 174.1 (C–S), 171.6 (C–O), 137.9, 132.2, 132.0, 131.2, 130.3, 127.7 (C₆H₅), 59.7, 59.2 (CH₂–N), 27.1, 26.0 (CH), 20.3, 20.18 (CH₃).

2.3.3. [Ni(L3)₂] (3)

Yield: 70%. Pink. m.p. 192 °C. *Anal. Calc.* for C₄₄H₃₄Cl₄NiN₄O₂S₂ (%): C, 57.73; H, 3.74; N, 6.12; S, 7.01. Found: C, 57.68; H, 3.71; N, 6.15; S, 6.98%. UV–Vis (5% DMF in buffer): λ_{max}, nm (ε, dm³ mol⁻¹ cm⁻¹) 245 (27360), 314 (39840), 386 (15200). FT–IR (KBr): ν, cm⁻¹ 1410 (C–O), 1242 (C–S). ¹H NMR (400 MHz, CDCl₃): δ, ppm 7.59–7.12 (m, 26H), 4.92 (s, 4H), 4.91 (s, 4H). ¹³C NMR (100 MHz, CDCl₃): δ, ppm 175.4 (C–S), 173.1 (C–O), 136.3, 136.1, 135.1, 133.8, 132.6, 131.7, 128.9, 128.8, 127.9, 127.6 (C₆H₅), 53.4, 52.0 (CH₂).

2.3.4. [Ni(L4)₂] (4)

Yield: 65%. Pink. m.p. 194 °C. *Anal. Calc.* for C₄₀H₂₆Cl₄NiN₄O₂S₂ (%): C, 55.91; H, 3.05; N, 6.52; S, 7.46. Found: C, 55.93; H, 3.07; N, 6.48; S, 7.42%. UV–Vis (5% DMF in buffer): λ_{max}, nm (ε, dm³ mol⁻¹ cm⁻¹) 241 (35520), 282 (52800), 398 (16560). FT–IR (KBr): ν, cm⁻¹ 1413 (C–O), 1301 (C–S). ¹H NMR (400 MHz, CDCl₃): δ, ppm 7.67–7.23 (m, 26H). ¹³C NMR (100 MHz, CDCl₃): δ, ppm 174.1 (C–S), 172.5 (C–O), 138.2, 132.2, 131.7, 131.6, 130.5, 129.1, 128.9, 128.4, 127.9, 127.8 (C₆H₅).

2.3.5. [Ni(L5)₂] (5)

Yield: 72%. Dark brown. m.p. 178 °C. *Anal. Calc.* for C₃₂H₄₂Cl₄NiN₄O₂S₂ (%): C, 49.32; H, 5.43; N, 7.19; S, 8.23. Found: C, 49.28; H, 5.46; N, 7.16; S, 8.00%. UV–Vis (5% DMF in buffer): λ_{max}, nm (ε, dm³ mol⁻¹ cm⁻¹) 242 (29840), 284 (40120), 392 (16880). FT–IR (KBr): ν, cm⁻¹ 1412 (C–O), 1148 (C–S). ¹H NMR (400 MHz, CDCl₃): δ, ppm 7.65 (d, *J* = 8.4 Hz, 2H), 7.33 (d, *J* = 1.6 Hz, 2H), 7.18–7.16 (dd, *J* = 8.4 & 1.6 Hz, 2H), 3.68–3.63 (m, 8H), 1.71–1.52 (m, 8H), 1.39–1.24 (m, 8H), 0.97–0.93 (t, *J* = 7.2 Hz, 6H), 0.90–0.86 (t, *J* = 7.2 Hz, 6H). ¹³C NMR (100 MHz, CDCl₃): δ, ppm 172.8 (C–S), 171.7 (C–O), 135.7, 135.2, 133.4, 132.2, 130.3, 126.4 (C₆H₅), 51.6, 50.9 (CH₂–N), 30.1, 29.2, 20.2, 20.1 (CH₂), 13.8 (CH₃).

2.3.6. [Ni(L6)₂] (6)

Yield: 64%. Brown. m.p. 170 °C. *Anal. Calc.* for C₂₈H₃₄Cl₄NiN₄O₂S₂ (%): C, 46.50; H, 4.74; N, 7.75; S, 8.87. Found: C, 46.47; H, 4.56; N, 7.59; S, 8.81%. UV–Vis (5% DMF in buffer): λ_{max}, nm (ε, dm³ mol⁻¹ cm⁻¹) 246 (26240), 288 (38150), 376 (15478). FT–IR (KBr): ν, cm⁻¹ 1412 (C–O), 1198 (C–S). ¹H NMR (400 MHz, CDCl₃): δ, ppm 7.50 (d, *J* = 7.6 Hz, 2H), 7.32 (d, *J* = 1.2 Hz, 2H), 7.16–7.15 (dd, *J* = 7.6 & 1.2 Hz, 2H), 3.76–3.45 (m, 4H), 1.38–1.19 (m, 24H). ¹³C NMR (100 MHz, CDCl₃): δ, ppm 172.4 (C–S), 171.5 (C–O), 136.0, 135.1, 131.0, 130.9, 130.2, 126.3 (C₆H₅), 65.8, 52.7 (CH), 20.0, 19.8 (CH₃).

2.4. Single crystal X-ray diffraction studies

A Bruker APEX2 X-ray (three-circle) diffractometer was employed for crystal screening, unit cell determination, and data collection. The X-ray radiation employed was generated from a Mo sealed X-ray tube (K_{α} = 0.70173 Å with a potential of 40 kV and a

current of 40 mA) fitted with a graphite monochromator in the parallel mode (175 mm collimator with 0.5 mm pinholes). Sixty data frames were taken at widths of 0.5°. These reflections were used in the auto-indexing procedure to determine the unit cell. A suitable cell was found and refined by nonlinear least squares and Bravais lattice procedures. The unit cell was verified by examination of the *hkl* overlays on several frames of data by comparing with both the orientation matrices. No super-cell or erroneous reflections were observed. After careful examination of the unit cell, a standard data collection procedure was initiated using omega scans. Integrated intensity information for each reflection was obtained by reduction of the data frames with the program APEX2 [44]. The integration method employed a three dimensional profiling algorithm and all data were corrected for Lorentz and polarization factors, as well as for crystal decay effects. Finally the data were merged and scaled to produce a suitable data set. The absorption correction program SADABS [45] was employed to correct the data for absorption effects. Systematic reflection conditions and statistical tests of the data suggested the space group. Solution was obtained readily using SHELXTL (XS) [46]. Hydrogen atoms were placed in idealized positions and were set riding on the respective parent atoms. All non-hydrogen atoms were refined with anisotropic thermal parameters. The structure was refined (weighted least squares refinement on F^2) to convergence [46,47]. Olex2 was employed for the final data presentation and structure plots [47]. The crystal data and refinement details of ligands (HL1, HL2 and HL3) and complexes (2 and 5) are listed in Table 1 and 2 respectively.

2.5. DNA binding studies

The experiments of DNA binding with the complexes were carried out in Tris–HCl/NaCl buffer solution (pH 7.2). Concentrated stock solutions of CT DNA were prepared in a 5 mM Tris–HCl/50 mM NaCl buffer and sonicated for 25 cycles, where each cycle consisted of 30 s with 1 min intervals. The absorption ratio of CT DNA solutions at λ_{max} 260 and 280 nm was found as 1.9:1. It showed that DNA was sufficiently free from protein impurities [48]. The concentration of DNA was determined using UV–Visible absorbance and the molar absorption coefficient (6600 M⁻¹ cm⁻¹) values at 260 nm [49]. The absorption titrations of the complexes (25 μM in Tris–HCl buffer containing 0.01% DMF) against CT DNA were performed by monitoring their absorption spectra with incremental addition of CT DNA within 0–50 μM concentration. The spectra were recorded after equilibration for 3 minutes, allowing the complexes to bind to the CT DNA. Concentrated stock solutions of the nickel(II) complexes (2–5) were prepared by dissolving calculated amounts of the complexes in a 5% DMF/5 mM Tris–HCl/50 mM NaCl buffer to required concentrations for all the experiments.

2.6. Competitive binding with ethidium bromide (EB)

The apparent binding constant (K_{app}) and quenching constant (K_q) values of the complexes (2–5) were determined by a fluorescence spectral technique using EB-bound CT DNA solution in Tris–HCl buffer (pH 7.2). The changes in fluorescence intensities at 596 nm (510 nm excitation) of EB bound to DNA were recorded with an increasing amount of the nickel(II) complex concentration until maximum reduction in the intensity of fluorescence occurred. In the presence of CT DNA, EB showed enhanced emission intensity due to its intercalative binding to DNA. A competitive binding of the nickel(II) complexes to CT DNA resulted in the displacement of the bound EB and decrease of its emission intensity [50].

Table 1
Crystal data and structure refinement for ligands.

Compound	HL1	HL2	HL3
Empirical formula	C ₁₂ H ₁₄ Cl ₂ N ₂ OS	C ₁₆ H ₂₂ Cl ₂ N ₂ OS	C ₂₃ H _{19.50} Cl ₂ N _{2.50} OS
Formula weight	305.21	361.32	449.87
T (K)	150(2)	110(2)	110(2)
Wavelength (Å)	0.71073	0.71073	0.71073
Crystal system	monoclinic	triclinic	triclinic
Space group	P2(1)/c	P $\bar{1}$	P $\bar{1}$
<i>Unit cell dimensions</i>			
a (Å)	14.225(5)	8.113(3)	10.136(7)
b (Å)	10.617(4)	10.561(4)	11.864(8)
c (Å)	9.986(3)	11.708(4)	18.820(13)
α (°)	90	107.538(4)	102.749(7)
β (°)	108.166(4)	108.655(4)	96.811(8)
γ (°)	90	98.420(3)	102.727(8)
V (Å ³)	1432.9(8)	872.9(5)	2120(2)
Z	4	2	4
D _{calc} (Mg/m ³)	1.415	1.375	1.410
Absorption coefficient (mm ⁻¹)	0.588	0.494	0.424
F(000)	632	380	932
Crystal size (mm ³)	0.64 × 0.45 × 0.09	0.48 × 0.42 × 0.38	0.56 × 0.40 × 0.40
θ Range for data collection (°)	2.44–27.50	2.10–27.49	1.13–27.50
Index ranges	–18 ≤ h ≤ 18, –13 ≤ k ≤ 13, –12 ≤ l ≤ 12	–10 ≤ h ≤ 10, –13 ≤ k ≤ 13, –15 ≤ l ≤ 15	–13 ≤ h ≤ 13, –15 ≤ k ≤ 15, –24 ≤ l ≤ 24
Reflections collected	23021	10062	24513
Independent reflections (R _{int})	3264 (0.0298)	3953 (0.0157)	9594 (0.0178)
Completeness to theta = 27.50° (%)	99.2	98.5	98.6
Absorption correction	semi-empirical from equivalents	semi-empirical from equivalents	semi-empirical from equivalents
Maximum and minimum transmission	0.9490 and 0.7047	0.8344 and 0.7973	0.8487 and 0.7972
Refinement method		full-matrix least-squares on F ²	
Data/restraints/parameters	3264/0/165	3953/0/203	9594/0/533
Goodness-of-fit (GOF) on F ²	1.029	1.059	1.026
Final R indices [I > 2σ(I)]	R ₁ = 0.0257, wR ₂ = 0.0646	R ₁ = 0.0262, wR ₂ = 0.0680	R ₁ = 0.0314, wR ₂ = 0.0770
R indices (all data)	R ₁ = 0.0298, wR ₂ = 0.0676	R ₁ = 0.0290, wR ₂ = 0.0693	R ₁ = 0.0353, wR ₂ = 0.0791
Largest difference in peak and hole (e Å ⁻³)	0.274 and –0.243	0.393 and –0.205	0.738 and –0.627

Table 2
Crystal data and structure refinement for complexes.

Compound	2	5
Empirical formula	C ₃₂ H ₄₂ Cl ₄ N ₄ NiO ₂ S ₂	C ₃₂ H ₄₂ Cl ₄ N ₄ NiO ₂ S ₂
Formula weight	779.33	779.33
T (K)	110(2)	110(2)
Wavelength (Å)	0.71073	0.71073
Crystal system	triclinic	monoclinic
Space group	P $\bar{1}$	P2(1)/c
<i>Unit cell dimensions</i>		
a (Å)	8.919(4)	8.6176(14)
b (Å)	14.858(7)	16.711(3)
c (Å)	15.272(7)	25.336(4)
α (°)	71.740(5)	90
β (°)	75.954(5)	95.928(2)
γ (°)	77.447(5)	90
V (Å ³)	1842.5(14)	3629.2(10)
Z	2	4
D _{calc} (Mg/m ³)	1.405	1.426
Absorption coefficient (mm ⁻¹)	0.964	0.979
F(000)	812	1624
Crystal size (mm ³)	0.58 × 0.40 × 0.18	0.58 × 0.58 × 0.35
θ Range for data collection (°)	2.31–27.49	2.02–27.50
Index ranges	–11 ≤ h ≤ 11, –19 ≤ k ≤ 19, –19 ≤ l ≤ 19	–11 ≤ h ≤ 11, –21 ≤ k ≤ 21, –32 ≤ l ≤ 31
Reflections collected	21505	35094
Independent reflections (R _{int})	8346 (0.0283)	8322 (0.0306)
Completeness to theta = 27.49° (%)	98.6	99.9
Absorption correction	semi-empirical from equivalents	semi-empirical from equivalents
Maximum and minimum transmission	0.8456 and 0.6047	0.7256 and 0.6005
Refinement method	full-matrix least-squares on F ²	full-matrix least-squares on F ²
Data/restraints/parameters	8346/9/426	8322/0/410
Goodness-of-fit on F ²	1.061	1.077
Final R indices [I > 2σ(I)]	R ₁ = 0.0357, wR ₂ = 0.0837	R ₁ = 0.0313, wR ₂ = 0.0670
R indices (all data)	R ₁ = 0.0442, wR ₂ = 0.0873	R ₁ = 0.0367, wR ₂ = 0.0688
Largest difference in peak and hole (e Å ⁻³)	1.435 and –0.434	0.289 and –0.367

2.7. Protein interaction studies

The excitation wavelength of BSA at 280 nm and the emission at 344 nm were monitored for the protein binding studies using fluorescence spectra recorded with nickel(II) complexes (**2–5**). The excitation and emission slit widths, and scan rates were constantly maintained for all the experiments. Samples were carefully degassed using pure nitrogen gas for 15 min by using quartz cells ($4 \times 1 \times 1 \text{ cm}^3$) with high vacuum Teflon stopcocks. Stock solution of BSA was prepared with phosphate buffer (50 mM, pH 7.2) and stored in dark at 4 °C for further use. Concentrated stock solutions of each test compound were prepared by dissolving them in DMF-phosphate buffer (5:95) and diluted with phosphate buffer to get required concentrations. 2.5 ml of BSA solution (1 μM) was titrated by successive additions of a 10^{-6} M stock solution of the complexes using a micropipette. Synchronous fluorescence spectra were also recorded using the same concentration of BSA and the complexes as mentioned above with two different $\Delta\lambda$ (difference between the excitation and emission wavelengths of BSA) values such as 15 and 60 nm.

2.8. MTT assay

MTT [3-(4,5-dimethylthiazole-2-yl)-2,5-diphenyl tetrazolium] assay was performed to evaluate the viability of the cells due to the effect of the samples tested and it is a colorimetric test based on the selective ability of viable cells to reduce the tetrazolium component of MTT in to purple colored formazan crystals. Two different dilutions were prepared by dilution with DMSO and media. To test the biocompatibility of the samples, cells were seeded at a density of 10000 cells/well into a 96 well plate. After attaining 90% confluency, the cells were incubated with different concentration of the samples for a period of 24 h. Cells in media alone devoid of test samples acted as a positive control and wells treated with Triton X-100 (1%) as a negative control. The cells were incubated with MTT solution for 4 h followed by 1 h incubation with solubilisation buffer. Then the absorbance of the solution was measured at a wavelength of 570 nm using a Beckmann Coulter Elisa plate reader (BioTek Power Wave XS). Triplicate samples were analyzed for each experiment. Cell viability was expressed as the percentage of the negative control calculated as, $\text{Viability (\%)} = (\text{Nt}/\text{Nc}) \times 100$;

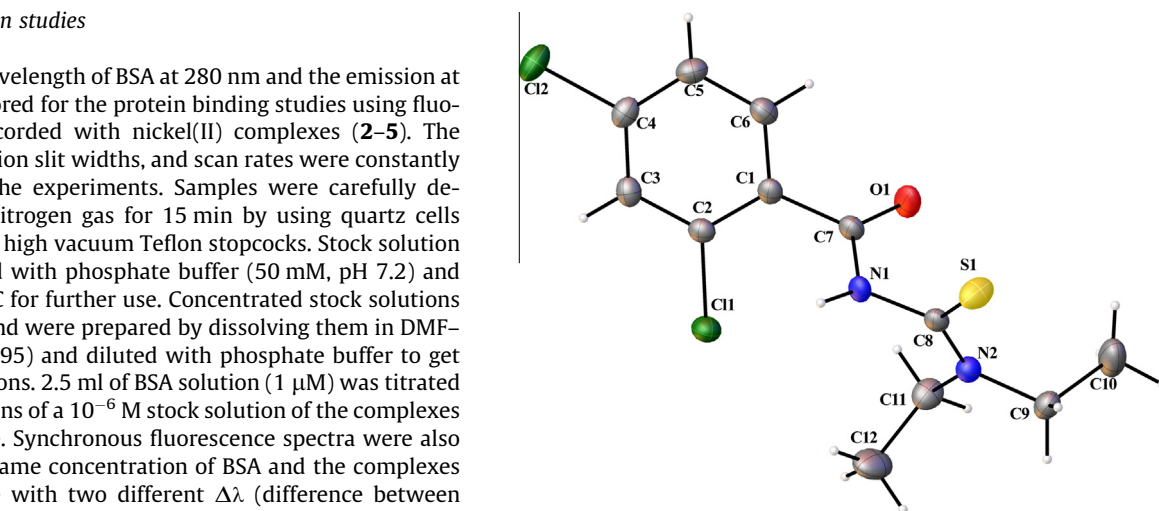


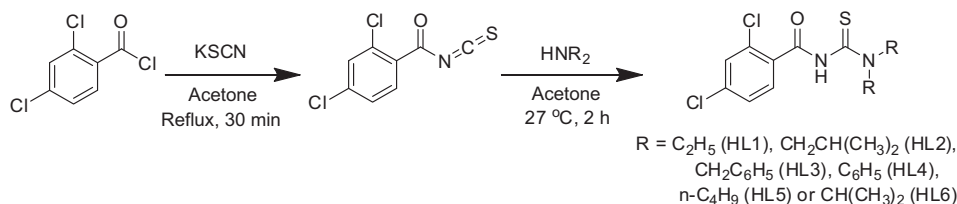
Fig. 1. Molecular structure of HL1.

Nt is the absorbance of the cells treated with sample and Nc is the absorbance of the untreated cells.

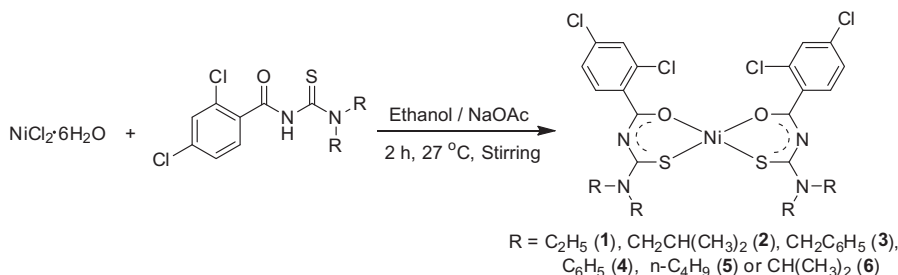
3. Results and discussion

3.1. Synthesis

Dichloro substituted benzoyl thiourea ligands were synthesized from 2,4-dichlorobenzoyl chloride, potassium thiocyanate and the corresponding secondary amine in acetone (Scheme 1). The square planar nickel(II) complexes were synthesized from the reactions between $\text{NiCl}_2 \cdot 6\text{H}_2\text{O}$ and the ligands in ethanol (Scheme 2). All the ligands and their corresponding complexes were obtained in good yield and were characterized by elemental analyses, and UV–Vis, FT-IR, ^1H and ^{13}C NMR spectroscopic techniques. The structures of the representative compounds were confirmed by single crystal X-ray diffraction studies. Investigations showed that 3,3-dialkyl/aryl-1-(2,4-dichlorobenzoyl)thioureas act as mono anionic bidentate ligands in the present case.



Scheme 1. Synthesis of ligands.



Scheme 2. Synthesis of Ni(II) complexes.

3.2. Spectroscopy

The electronic spectra of the complexes measured in 5% DMF in buffer showed three bands in the regions 241–247, 282–314 and 382–398 nm, which were assigned to intra ligand, charge-transfer ($L \rightarrow M$), and forbidden $d \rightarrow d$ transitions respectively. In the FT-IR spectra of all the ligands, bands were observed at 1654–1702 and 1222–1265 cm^{-1} , which were assigned to $C=O$ and $C=S$ stretching vibrations respectively. These bands underwent a shift after coordination of the ligands with nickel *via* O and S donor atoms and appeared respectively at 1376–1440 and 1157–1243 cm^{-1} in the spectra of the complexes. The FT-IR spectra of the acylthiourea

ligands showed N-H stretching vibrations at 3161–3257 cm^{-1} , which disappeared in the corresponding nickel(II) complexes indicating enolization followed by deprotonation prior to coordination. This is consistent with the observation made in ^1H NMR spectral studies. The signals of the N-H protons were observed as singlet at δ 8.35–8.70 in the spectra of ligands, which disappeared in that of nickel(II) complexes. The resonances of aromatic and aliphatic protons of the ligands were appeared at δ 7.12–7.63 and δ 0.91–5.17 respectively. The signals due to aromatic and aliphatic protons did not undergo a significant shift in the nickel(II) complexes. The occurrence of sharp and non-shifted peaks in the ^1H NMR spectra of all the complexes reveals the diamagnetic

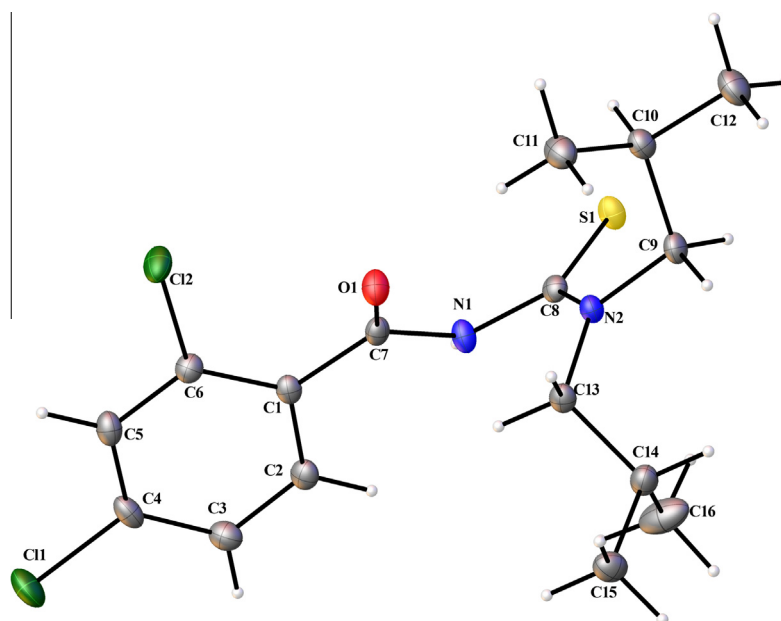


Fig. 2. Molecular structure of HL2. (The amide hydrogen is eclipsed behind the nitrogen atom)

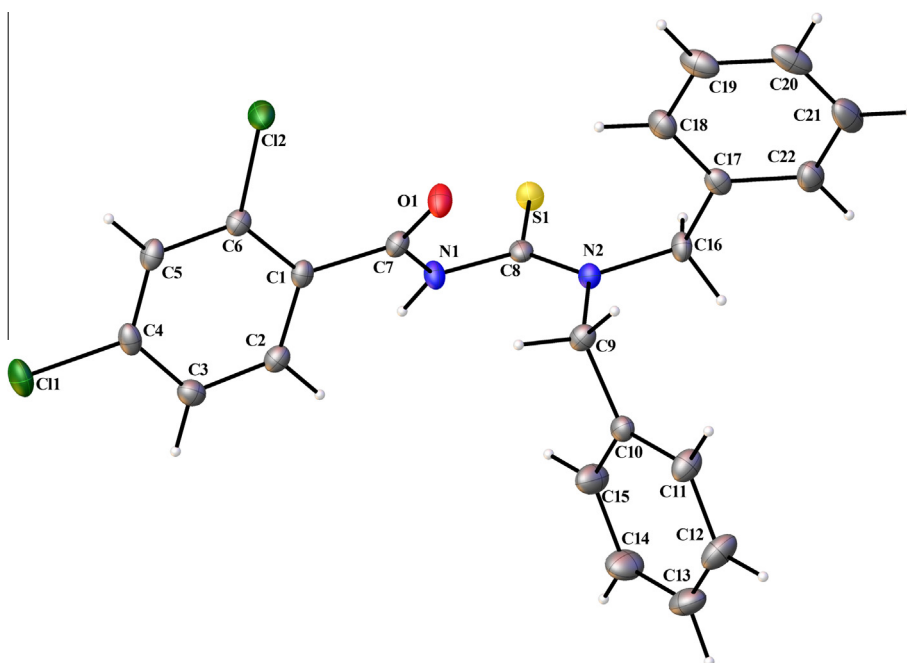


Fig. 3. Molecular structure of HL3.

nature of the low-spin Ni(II) (d^8) ion with a square planar geometry. The resonances due to carbons in the ^{13}C NMR spectra of the ligands and the complexes were observed in the expected regions.

3.3. Crystal structures

The ORTEP diagrams of ligands (HL1, HL2 and HL3) and complexes (**2** and **5**) with the atomic labeling schemes are shown in

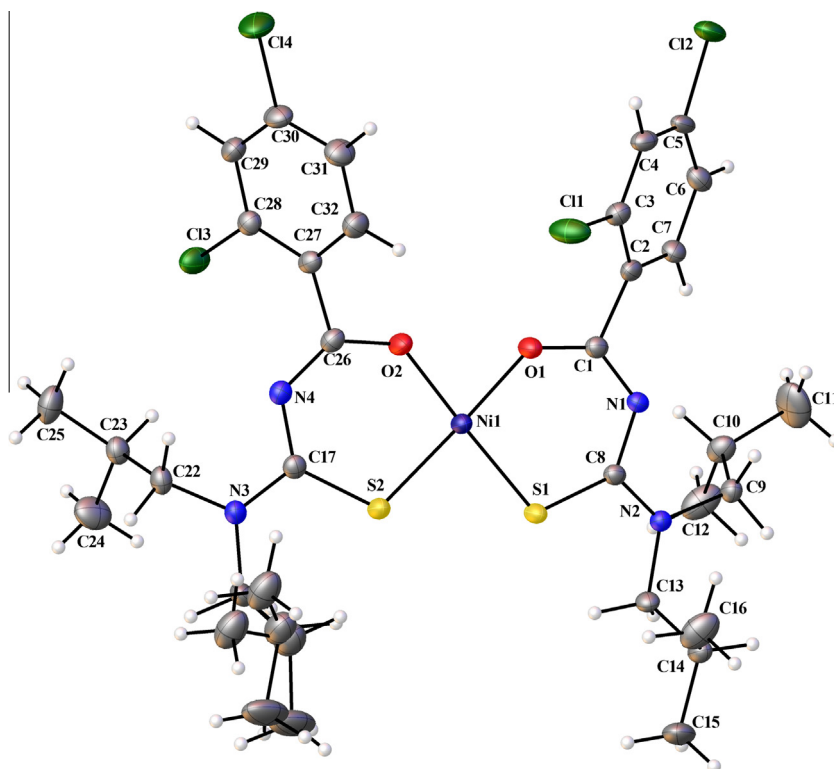


Fig. 4. Molecular structure of **2**.

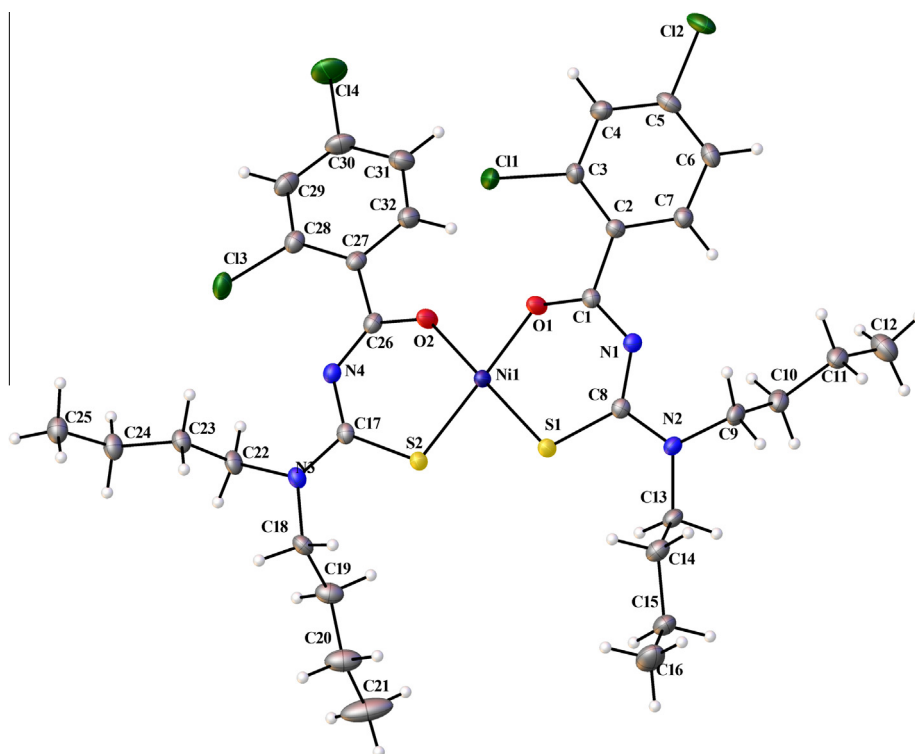


Fig. 5. Molecular structure of **5**.

the Figs. 1–5. Selected interatomic bond lengths and bond angles are in Table 3. Half a molecule of CH_3CN was found solvated per molecule of the HL3. C19–C21 atoms in **5** were found disordered between two positions and were modeled successfully with a ratio of 0.74:0.26. Structural analysis revealed that **2** and **5** have a square planar geometry with a *cis*- NiO_2S_2 chromophore, in which two acylthiourea (HL) ligands were coordinated to nickel centre as mono anionic bidentate ligands. Further, the structural index value (τ_4)

for **2** is 0.028, and for **5** it is 0.0196, suggesting square planar geometry around Ni [51]. Comparing the C–O and C–S bond lengths of **2** with HL2, there was a considerable elongation of these bonds in the complex. On the other hand, N–C bonds of the chelate rings in **2** were short compared to the N–C bond distances of the corresponding ligand. These results are consistent with the fact that the ligand underwent deprotonation during the reaction and coordinated to nickel ion *via* O and S donor atoms. Further, there was a significant

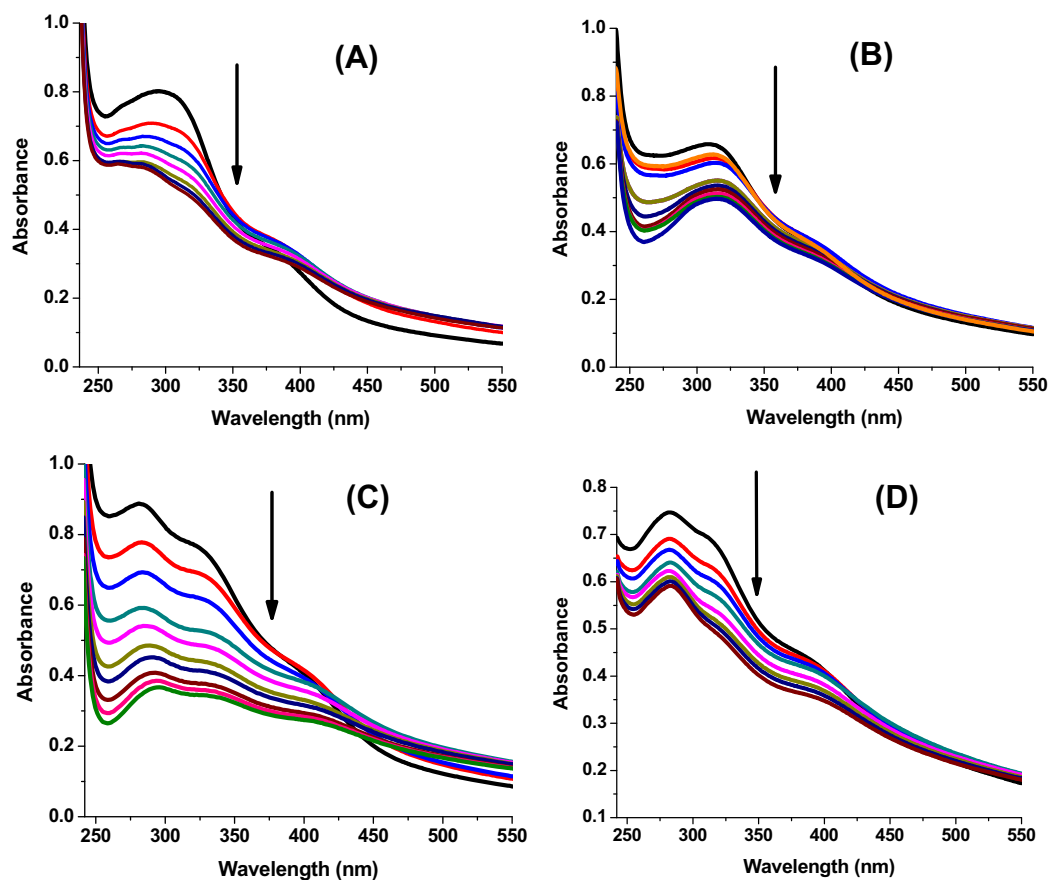


Fig. 6. Absorption spectra of complexes **2** (A), **3** (B), **4** (C) and **5** (D) in Tris-HCl buffer upon addition of CT-DNA. [Complex] = 2.5×10^{-5} M, [DNA] = 0–50 μM . Arrow shows that the absorbance intensities decrease upon increasing DNA concentration.

Table 3
Selected bond lengths (\AA) and angles ($^\circ$).

Ligand	HL1	HL2	HL3	Complex	2	5
Cl(1)–C(4)	1.7367(14)	1.7317(13)	1.7338(17)	Ni(1)–O(1)	1.8500(16)	1.8609(12)
S(1)–C(8)	1.6670(13)	1.6819(12)	1.6796(16)	Ni(1)–O(2)	1.8535(15)	1.8459(12)
O(1)–C(7)	1.2283(14)	1.2107(15)	1.2088(18)	Ni(1)–S(2)	2.1391(11)	2.1322(5)
N(1)–C(7)	1.3486(15)	1.3906(15)	1.3868(18)	Ni(1)–S(1)	2.1472(9)	2.1426(5)
N(1)–C(8)	1.4343(15)	1.4057(15)	1.4032(19)	Cl(1)–C(3)	1.739(2)	1.7311(17)
N(1)–H(1)	0.8470	0.8999	0.8800	S(1)–C(8)	1.737(2)	1.7271(17)
N(2)–C(8)	1.3245(16)	1.3263(15)	1.3271(19)	O(1)–C(1)	1.263(2)	1.2633(19)
N(2)–C(9)	1.4655(16)	1.4750(15)	1.4740(18)	N(1)–C(1)	1.319(2)	1.318(2)
N(2)–C(11,13, 16)	1.4783(16)	1.4776(15)	1.4646(18)	N(1)–C(8)	1.352(2)	1.345(2)
C(7)–N(1)–C(8)	121.70(9)	122.28(10)	123.10(12)	O(1)–Ni(1)–O(2)	83.30(6)	83.73(5)
C(8)–N(1)–H(1)	117.0	118.5	118.5	O(1)–Ni(1)–S(2)	177.89(5)	177.63(4)
C(8)–N(2)–C(9)	121.22(10)	120.10	124.87(12)	O(2)–Ni(1)–S(2)	94.89(5)	94.25(4)
C(9)–N(2)–C(11)	115.30(10)	115.31(9)	120.94(11)	O(1)–Ni(1)–S(1)	94.89(5)	95.89(4)
C(1,5)–C(2,4)–Cl(1)	120.80(9)	118.39(9)	118.56(12)	O(2)–Ni(1)–S(1)	178.06(5)	179.61(4)
O(1)–C(7)–N(1)	122.64(11)	122.54(11)	122.54(13)	S(2)–Ni(1)–S(1)	86.93(3)	86.13(2)
O(1)–C(7)–C(1)	121.00(11)	122.60(10)	124.04(13)	C(8)–S(1)–Ni(1)	108.78(7)	108.10(6)
N(1)–C(7)–C(1)	116.32(10)	114.73(10)	113.34(12)	C(17)–S(2)–Ni(1)	109.67(7)	109.32(6)
N(2)–C(8)–N(1)	115.15(11)	117.46(10)	116.92(12)	C(1)–O(1)–Ni(1)	133.38(13)	131.85(11)
N(2)–C(8)–S(1)	126.45(9)	124.14(9)	125.39(11)	C(26)–O(2)–Ni(1)	133.00(14)	134.42(11)
N(1)–C(8)–S(1)	118.38(9)	118.38(9)	117.67(10)			

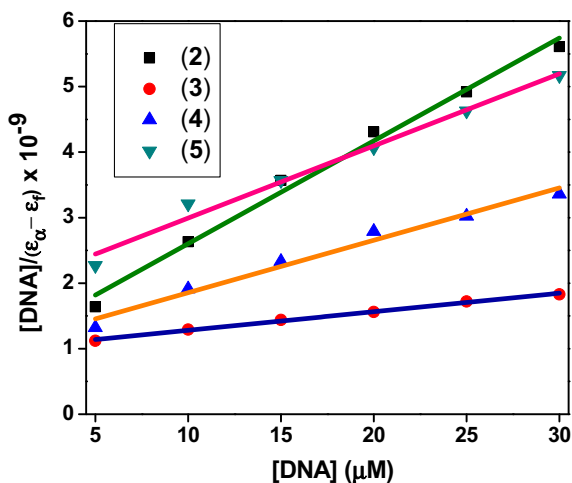


Fig. 7. Plots of $[DNA]/(\epsilon_a - \epsilon_f)$ vs. $[DNA]$ for the titration of the complexes with CT DNA.

delocalization of π -electron density over the six atoms comprising the respective chelate rings in the complex. The coordination geometries and bonding characteristics of **2** and **5** are similar to that of previously reported nickel(II) acylthiourea complexes [43].

3.4. DNA binding studies

3.4.1. Electronic absorption titration

Absorption titration technique has been used to monitor the mode of interaction of complexes (**2–5**) with CT DNA (Fig. 6) [52]. Upon the incremental addition of CT DNA to the complexes

the charge transfer band (282–314 nm) shows increasing hypochromism ($\Delta\epsilon$, 19–54%) with a small red shift. As the extent of hypochromism is commonly associated with the strength of DNA interaction, the observed decrease in order of hypochromism, $2 > 5 > 3 > 4$, reflects the decrease in DNA binding affinities of the complexes in this order. These results proposed association of the compounds with CT DNA, and it also probably that these compounds interact with the helix *via* intercalation. The DNA binding affinities of the complexes are compared quantitatively by obtaining the intrinsic binding constant K_b using the following equation:

$$[DNA]/(\epsilon_a - \epsilon_f) = [DNA]/(\epsilon_b - \epsilon_f) + 1/K_b(\epsilon_a - \epsilon_f)$$

where $[DNA]$ is the concentration of DNA in base-pairs, ϵ_a is the apparent extinction coefficient obtained by calculating absorbance/[complex], ϵ_f is the extinction coefficient of the complex in its free form, and ϵ_b is the extinction coefficient of the complex in the bound form. Each set of data, when fitted into the above equation, gave a straight line with a slope of $1/(\epsilon_b - \epsilon_f)$ and an intercept of $1/K_b(\epsilon_a - \epsilon_f)$ and the value of K_b was determined from the ratio of slope to intercept (Fig. 7). The observed K_b values (2.51 – $7.57 \times 10^4 \text{ M}^{-1}$, Table 4) of the nickel(II) complexes are higher than those of previously reported [53–56]. The complexes **2** ($K_b = 7.57 \times 10^4 \text{ M}^{-1}$) and **5** ($K_b = 5.62 \times 10^4 \text{ M}^{-1}$) showed higher DNA binding affinity than the complexes **3** ($K_b = 2.51 \times 10^4 \text{ M}^{-1}$) and **4** ($K_b = 2.91 \times 10^4 \text{ M}^{-1}$). Interestingly, the complex **2** showed better DNA binding property than the complex **5**; this may be due to the rigid nature of the isobutyl group, which favors stronger interaction with DNA [57].

3.4.2. Fluorescence spectroscopic studies

In an effort to understand the interaction pattern of the complexes with CT DNA more clearly, fluorometric competitive binding experiment was carried out using EB as a probe. The intrinsic

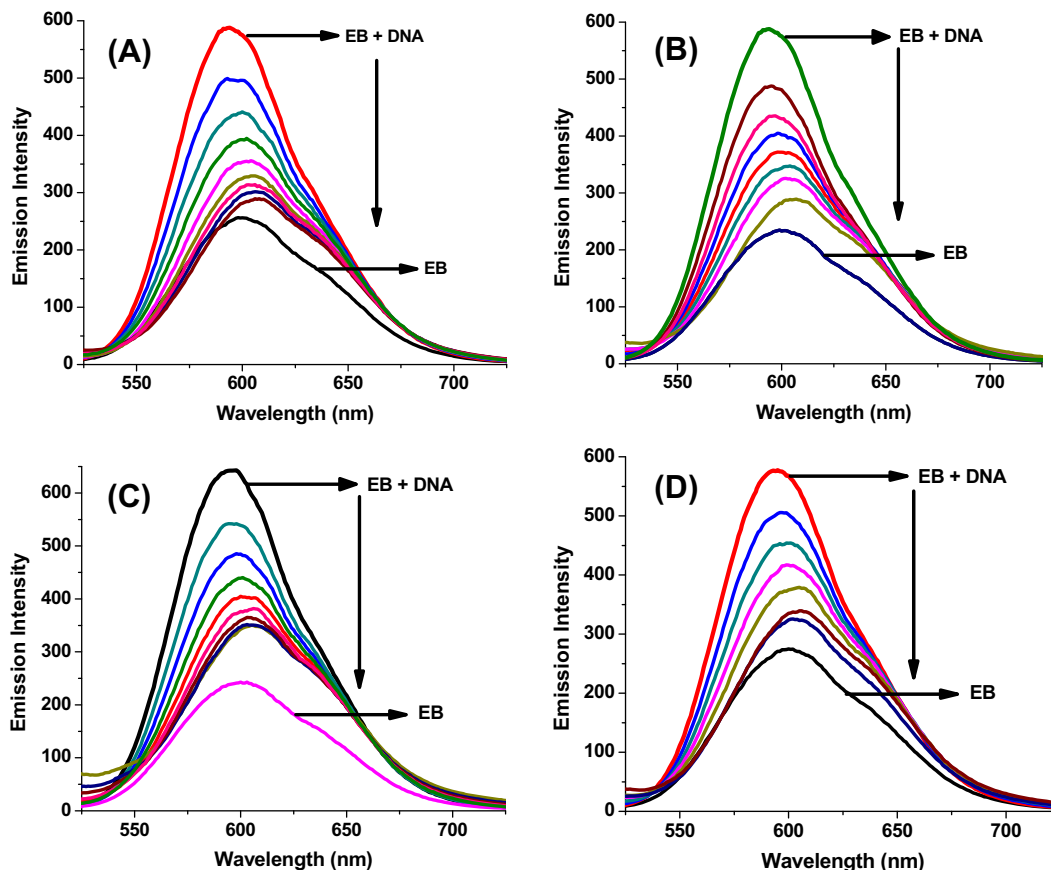


Fig. 8. Fluorescence quenching curves of EB bound to DNA in the presence of complexes **2** (A), **3** (B), **4** (C) and **5** (D). $[DNA] = 5 \mu\text{M}$, $[EB] = 5 \mu\text{M}$ and $[\text{complex}] = 0$ – $30 \mu\text{M}$.

Table 4
DNA binding constant (K_b), quenching constant (K_q) and apparent binding constant (K_{app}) values.

Complex	K_b (M^{-1})	K_q (M^{-1})	K_{app} (M^{-1})
2	7.57×10^4	2.86×10^4	1.43×10^6
3	2.51×10^4	2.16×10^4	1.08×10^6
4	2.91×10^4	2.19×10^4	1.09×10^6
5	5.62×10^4	2.69×10^4	1.35×10^6

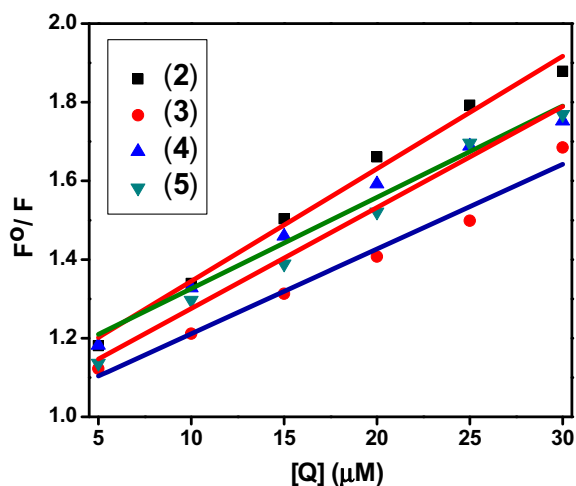


Fig. 9. Stern-Volmer plots of fluorescence titrations of the complexes with CT DNA.

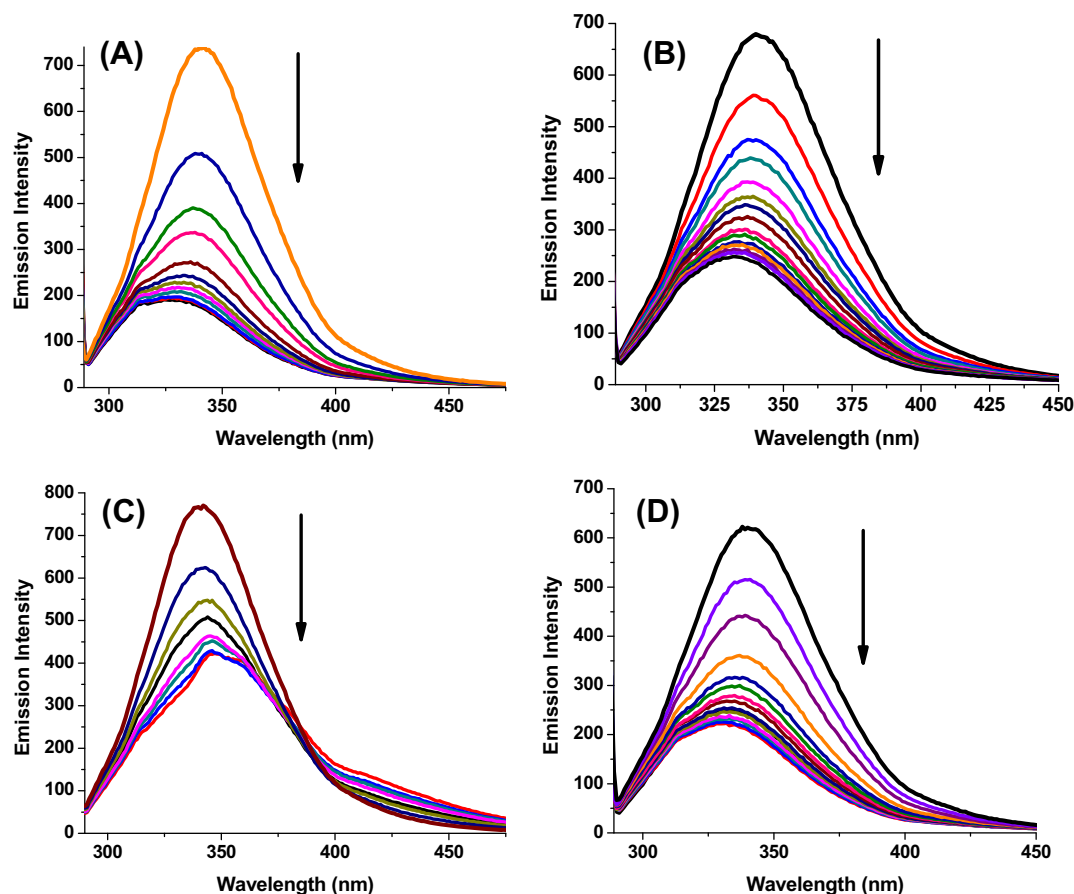


Fig. 10. Fluorescence quenching curves of BSA in the absence and presence of complexes 2 (A), 3 (B), 4 (C) and 5 (D). [BSA] = 1 μ M and [complex] = 0–30 μ M.

fluorescence intensities of DNA and that of EB in Tris–HCl buffer are low. However, EB emits intense fluorescent light in the presence of DNA due to its strong intercalation between the adjacent DNA base pairs [58,59]. If the complexes can intercalate into DNA, the binding sites of DNA available for EB will be decreased, hence the fluorescence intensity of EB will be quenched. This is a proof that the complexes intercalate between the base pairs of DNA [60,61]. The quenching extent of fluorescence of EB bound DNA was used to determine the extent of binding between the complex and DNA. The emission spectra of EB binding to DNA in the absence and presence of the complexes are given in Fig. 8. The addition of the complexes to DNA pretreated with EB causes an appreciable reduction in the emission intensity, indicating the replacement of EB by the complexes. The Stern–Volmer quenching constant [62] for each complex was calculated using the equation given as $F^0/F = 1 + K_q [Q]$. Here, F^0 and F are the fluorescence intensity in the absence and presence of complexes, respectively, K_q is a linear Stern–Volmer quenching constant, and $[Q]$ is the total concentration of a complex to that of DNA. The value of K_q is given by the ratio of slope to intercept in a plot of F^0/F versus $[Q]$ (Fig. 9). The quenching constant values are listed in Table 4. The apparent binding constant (K_{app}) values of DNA were calculated by using the equation $K_{EB} [EB] = K_{app} [\text{complex}]$, where the complex concentration is the values at 50% reduction in the fluorescence intensity of EB, K_{EB} ($1.0 \times 10^7 M^{-1}$) is the DNA binding constant of EB (Table 4). Complexes 2 and 5 represented a slightly more pronounced quenching effect on fluorescence intensity of EB and DNA, underscoring its tighter binding to DNA as compared to the rest of complexes (3 and 4). The observed quenching constant and binding constant values of the nickel(II) complexes proposed that the complexes interact with CT DNA through intercalation.

3.5. Protein binding studies

3.5.1. Fluorescence quenching of BSA by nickel(II) complexes

Bovine serum albumin (BSA) is the most extensively studied serum albumin, owing to its structural homology with human serum albumin (HSA). It is well known that the transport of drugs through the bloodstream is affected via the interaction of drugs with blood plasma proteins. Binding to these proteins may lead to loss or enhancement of the biological properties of the original compounds, or may provide paths for their transportation. Fluorescence quenching analyses are usually employed to analyze the interaction of chemical compounds with BSA. A solution of BSA (1 μM) was titrated with various concentrations of the complexes (0–30 μM). Fluorescence spectra were recorded in the range from 290 to 450 nm upon excitation at 280 nm. The effect of complexes (2–5) on the fluorescence spectrum of BSA is shown in Fig. 10. Upon the addition of the nickel(II) complexes to the solution of BSA, fluorescence intensity at 344 nm decreases up to 74.5%, 58.4%, 46.6% and 64.8%, from the initial intensity of BSA, accompanied by a hypsochromic shift of 6, 4 and 5 nm for complexes 2, 3 and 5 respectively, and bathochromic shift of 4 nm for complex 4. The observed hypochromicity with blue or red shift has revealed that the complexes interact hydrophobically with the BSA protein [63]. The fluorescence quenching data were analyzed by Stern–Volmer and Scatchard equations. The quenching constant (K_q) can be calculated using the plot of $\log (F^0/F)$ versus $\log [Q]$ (Fig. 11). If it is assumed that the binding of complexes with BSA occurs at equilibrium, the equilibrium binding constant can be analyzed according to the Scatchard equation $\log [(F^0-F)/F] = \log K_b + n \log [Q]$, where K_b is the binding constant of the compound with BSA and n is the number of binding sites. From the plot of $\log [(F^0-F)/F]$ versus $\log [Q]$ (Fig. 12), the number of binding sites (n) and the binding constant (K_b) values have been obtained. The calculated K_q , K_b and n values are given in Table 5. The calculated value of n is around 1 for all of the complexes. The values of K_q and K_b suggested the binding of complexes with BSA. Among the four complexes, complex 2 exhibited better interaction with BSA compared to other complexes (3, 4 and 5).

Generally, quenching occurs through either dynamic or static mode. The dynamic quenching is a process in which the fluorophore and the quencher come into contact during the transient existence of the excited state, whereas static quenching refers to the formation of fluorophore–quencher complex in the ground state. The easiest method to determine the type of quenching is

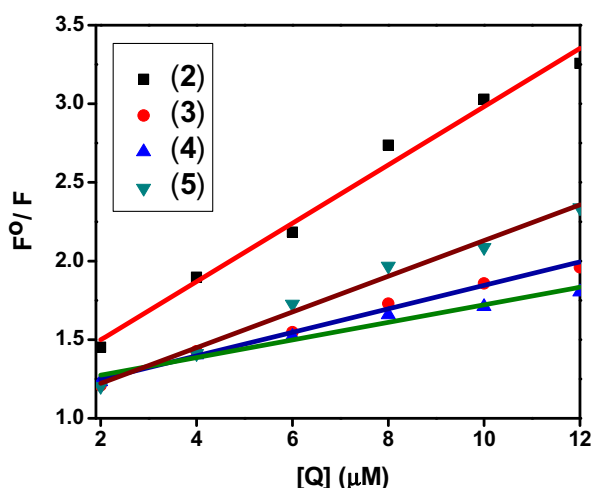


Fig. 11. Stern–Volmer plots of the fluorescence titrations of the complexes with BSA.

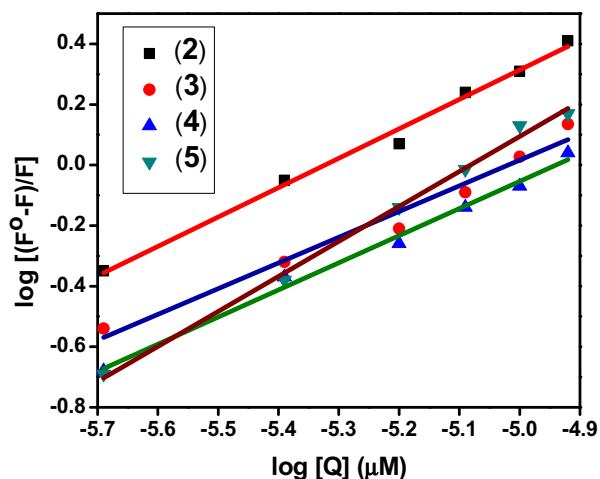


Fig. 12. Scatchard plots of the fluorescence titrations of the complexes with BSA.

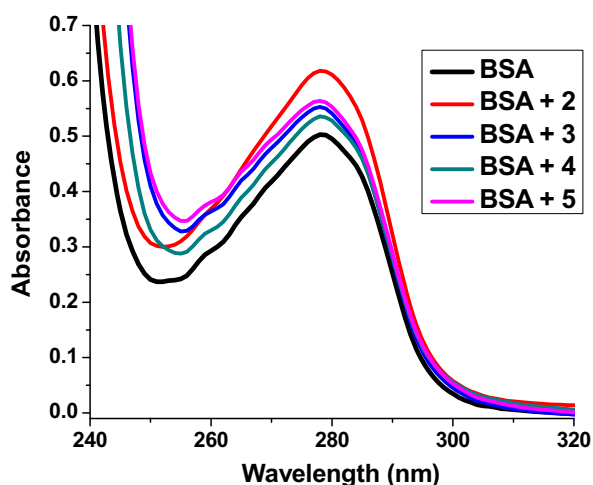


Fig. 13. The absorption spectra of BSA (10 μM) and BSA with complexes 2–5 (4 μM).

Table 5

Protein binding constant (K_b), quenching constant (K_q) and number of binding sites (n) values.

Complex	K_b (M^{-1})	K_q (M^{-1})	n
2	4.07×10^5	1.85×10^5	1.11
3	4.61×10^4	7.47×10^4	0.94
4	4.41×10^4	5.71×10^4	0.91
5	1.48×10^5	1.14×10^5	0.97

UV–Vis absorption spectroscopy. The UV–Vis spectra of BSA in the absence and the presence of complexes are shown in Fig. 13, which indicates that the addition of nickel(II) complexes to a fixed concentration of BSA led to a gradual increase in the intensity of BSA absorption but at the same wavelength due to the interaction between test compounds and protein. In other words, the fluorescence quenching between complexes and BSA is mainly ascribed to be static quenching [64]. The above results revealed the strong interaction between nickel(II) complexes and BSA that caused a change in the conformation of BSA.

3.5.2. Characteristics of synchronous fluorescence spectra

Synchronous fluorescence spectroscopy provides information on the molecular microenvironment, particularly in the vicinity

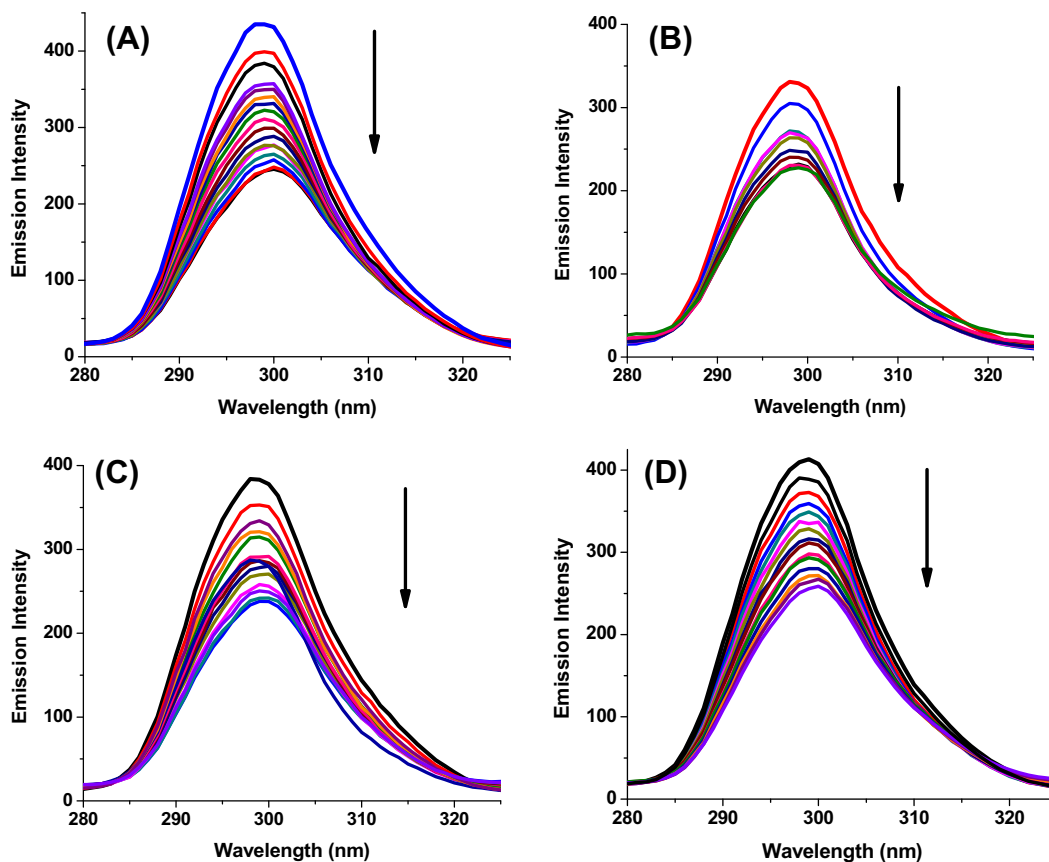


Fig. 14. Synchronous spectra of BSA (1 μM) as a function of concentration of the complexes 2 (A), 3 (B), 4 (C) and 5 (D) (0–30 μM) with $\Delta\lambda = 15$ nm.

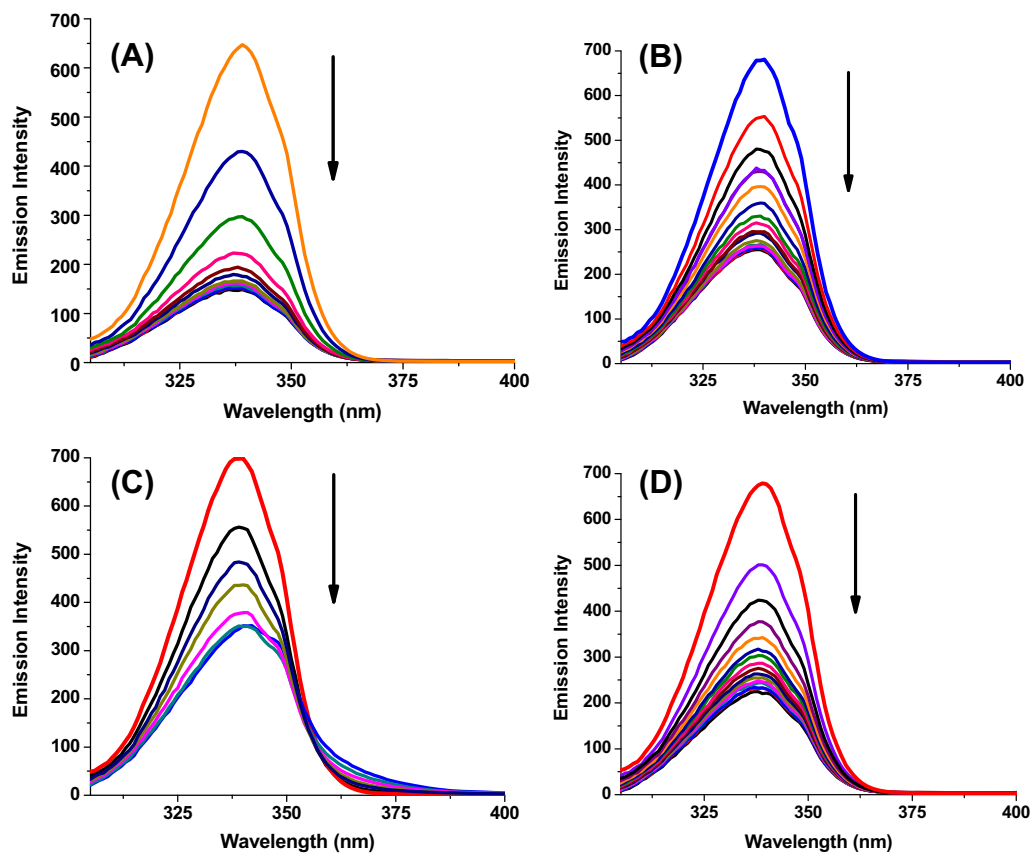


Fig. 15. Synchronous spectra of BSA (1 μM) as a function of concentration of the complexes 2 (A), 3 (B), 4 (C) and 5 (D) (0–30 μM) with $\Delta\lambda = 60$ nm.

of the fluorophore functional groups [65]. The fluorescence of BSA might be due to the presence of tyrosine, tryptophan and phenylalanine residues. According to Miller [66], the difference between excitation and emission wavelengths ($\Delta\lambda$) reflects the nature of chromophores. Large (~60 nm) and small (~15 nm) $\Delta\lambda$ values are characteristic of tryptophan and tyrosine residues respectively [67]. Synchronous fluorescence spectra of BSA were recorded at

both 15 and 60 nm $\Delta\lambda$ with the addition of the nickel(II) complexes (2–5) in various concentrations to understand the structural changes occurred in BSA (Figs. 14 and 15). While increasing the concentration of the complexes, the intensity of emission corresponding to tyrosine (at 302 nm) was found to decrease in the magnitude of 43.7%, 31.6%, 24.8% and 37.4% for complexes 2, 3, 4 and 5 respectively without any shift in emission wavelength. The

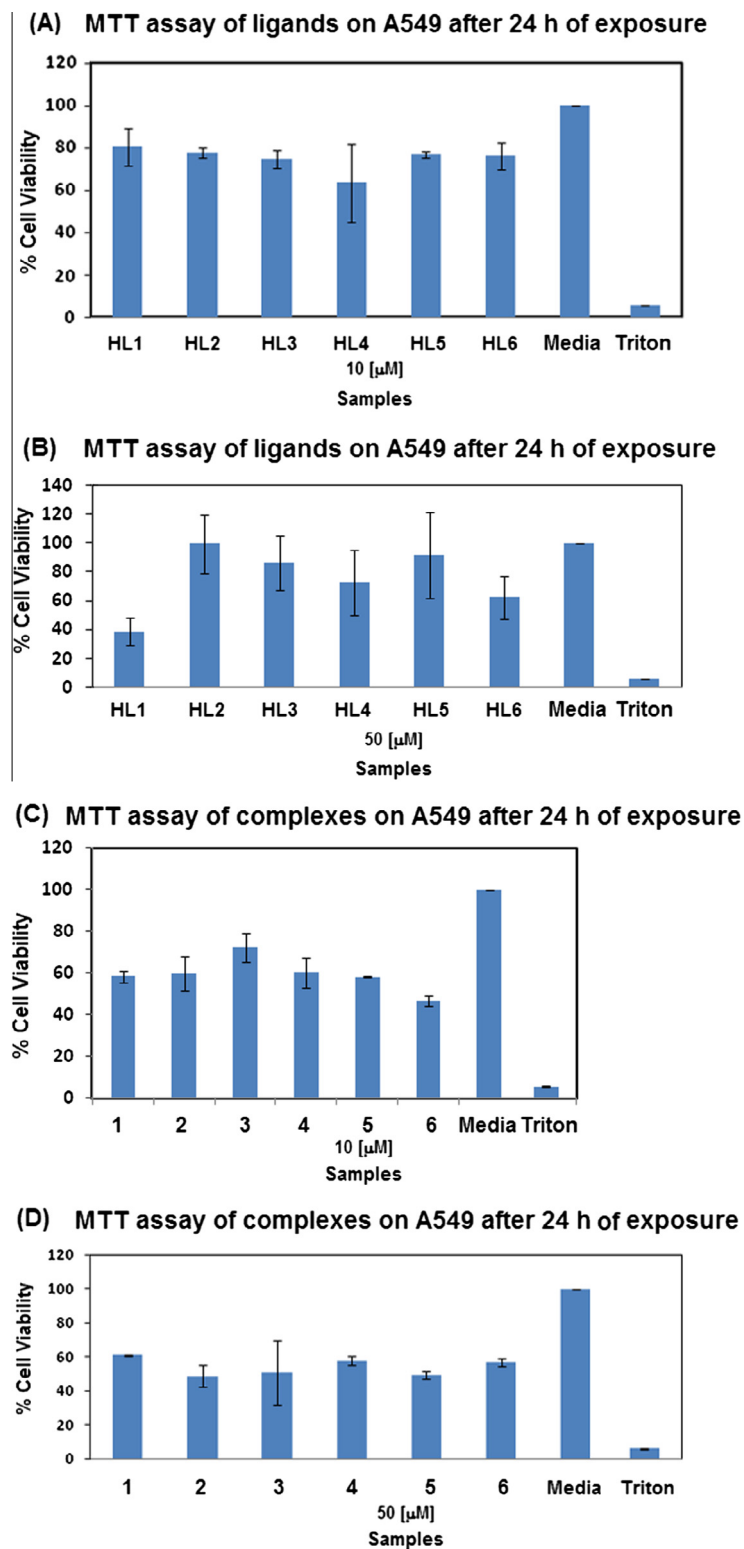


Fig. 16. Cytotoxicity of HL1–HL6 (A and B) and 1–6 (C and D) after 24 h incubation on A549 cell lines.

tryptophan fluorescence emission showed significant decrease in the intensity (at 342 nm) of about 77.5%, 62.7%, 50.4% and 66.8% for complexes **2**, **3**, **4** and **5** respectively, without any change in the position of the emission band. These experimental results indicate that although the complexes affected the microenvironments of both tyrosine and tryptophan during the binding process, the effect was more towards tryptophan than tyrosine.

3.6. Cytotoxic activity

The cytotoxicity of the ligands (HL1–HL6) and their nickel(II) complexes (**1**–**6**) toward A549 (human lung cancer) and HT29 cells (human colon adenocarcinoma) has been examined in comparison with cisplatin ($IC_{50} = 25 \mu\text{M}$) under identical conditions by using MTT assay [26]. Fig. 16 depicts the cytotoxic effect of the ligands

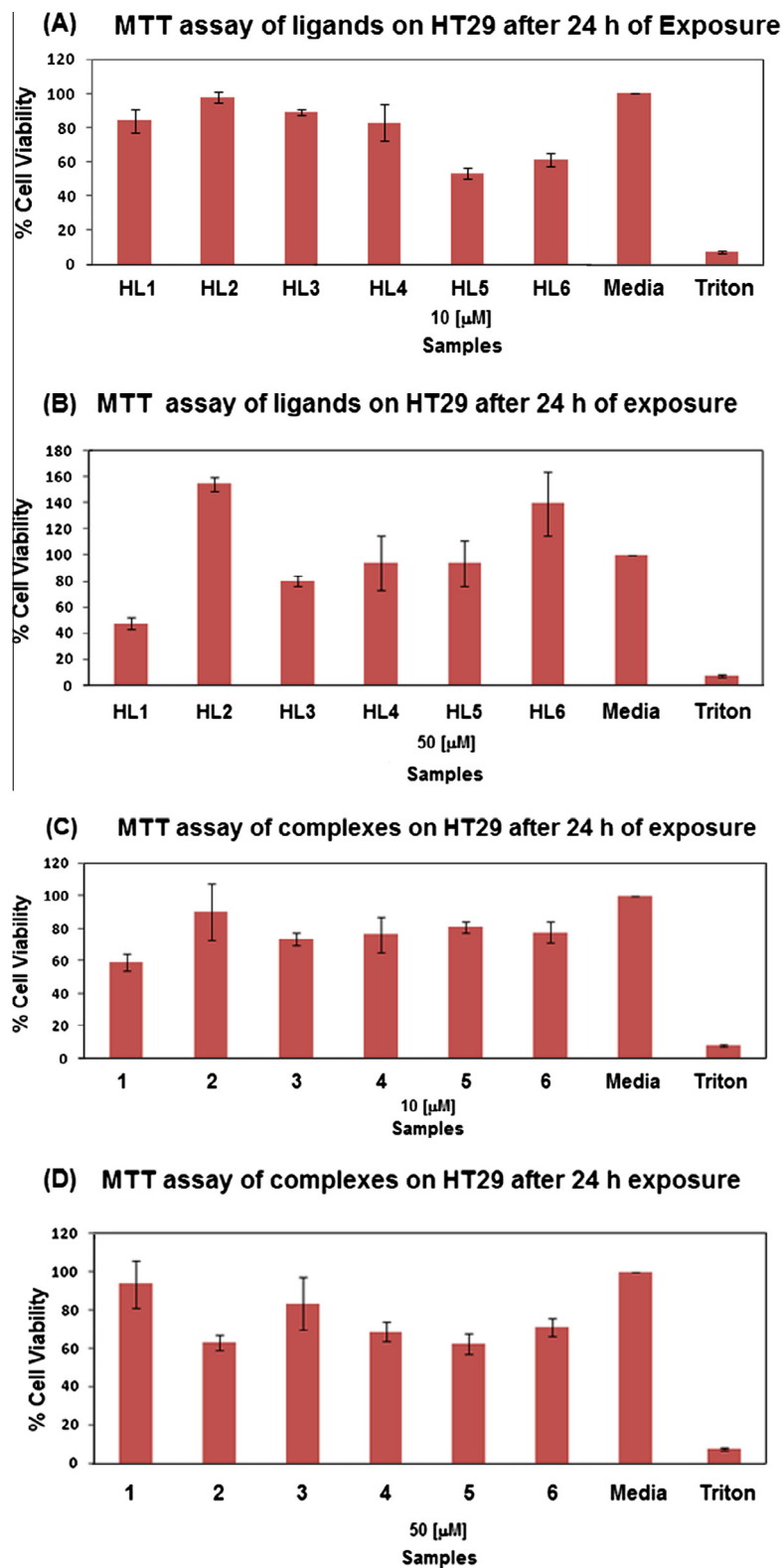


Fig. 17. Cytotoxicity of HL1–HL6 (A and B) and **1**–**6** (C and D) after 24 h incubation on HT29 cell lines.

(HL1–HL6) and nickel(II) complexes (**1–6**) after 24 h incubation on A549 cell lines. The IC50 value of **6** is 17.1 μM in low micromolar concentration (10 μM), which is higher than the other complexes studied. At high concentration (50 μM), complexes **2** and **5** possess a prominent cytotoxicity (IC50 = 29.2 and 26.3 μM for **2** and **5** respectively), which is consistent with their strong DNA and protein binding properties. Fig. 17 shows the cytotoxicity of the compounds (HL1–HL6 and **1–6**) after 24 h incubation on HT29 cell lines. Complex **1** exhibited higher activity (40% inhibition) than the other complexes (**2–6**) at 10 μM concentration. As expected, complexes **2** and **5** showed higher activity at 50 μM with inhibition values of 40% and 42% respectively. It has been observed that in few cases ligand exhibited higher cytotoxicity than the corresponding complex; particularly HL1 in higher concentration.

4. Conclusion

In conclusion, we have synthesized and characterized new nickel(II) complexes of 3,3-dialkyl/aryl-1-(2,4-dichlorobenzoyl)thiourea. UV–Vis and fluorescence spectral studies indicated the binding of the complexes with CT DNA. Fluorescence quenching experiments revealed the interaction of the complexes with BSA protein. The nickel(II) complexes also showed cytotoxicity against A549 and HT29 cell lines.

Acknowledgements

N.S. thanks NITT for the fellowship. We thank Dr. R. Jayakumar, Amrita Institute of Medical Sciences, Kochi for cytotoxicity experiments. R.K. gratefully acknowledges DST, India for the financial support under FIST programme.

Appendix A. Supplementary material

Crystallographic data for the structures reported in this paper have been deposited with the Cambridge Crystallographic Data Centre (CCDC) as supplementary publication numbers CCDC 949126, CCDC 949127, CCDC 949128, CCDC 949129 and CCDC 949130 for HL1, HL2, HL3, **2** and **5**, respectively. Copies of the data can be obtained free of charge from the CCDC (12 Union Road, Cambridge CB2 1EZ, UK; Tel.: +44-1223-336408; Fax: +44-1223-336003; e-mail: deposit@ccdc.cam.ac.uk; Web site <http://www.ccdc.cam.ac.uk>).

References

- [1] M.A. Fuertes, C. Alonso, J.M. Perez, *Chem. Rev.* 103 (2003) 645.
- [2] G. Gasser, I. Ott, N. Metzler-Nolte, *J. Med. Chem.* 54 (2011) 3.
- [3] S.J. Berners-Price, *Angew. Chem., Int. Ed. Engl.* 50 (2011) 804.
- [4] S.J. Berners-Price, A. Filipovska, *Metalomics* 3 (2011) 863.
- [5] I. Ott, *Coord. Chem. Rev.* 253 (2009) 1670.
- [6] C. Metcalfe, J.A. Thomas, *Chem. Soc. Rev.* 32 (2003) 215.
- [7] K.E. Erkkila, D.T. Odom, J.K. Barton, *Chem. Rev.* 99 (1999) 2777.
- [8] J.K. Barton, *Science* 233 (1986) 727.
- [9] B. Armitage, *Chem. Rev.* 98 (1998) 1171.
- [10] R. David, D.R. McMillin, K.M. McNett, *Chem. Rev.* 98 (1998) 1201.
- [11] H. Sigel, A. Sigel (Eds.), *Nickel and its role in biology in Metal Ions in Biological Systems*, 2004, vol. 23, Marcel Dekker, New York, 1988.
- [12] N.C. Kasuga, K. Sekino, C. Koumo, N. Shimada, M. Ishikawa, K. Nomiya, *J. Inorg. Biochem.* 84 (2001) 55.
- [13] M. Alexiou, V. Tsivikas, C. Dendrinou-Samara, A.A. Pantazaki, P. Trikalitis, N. Lalioti, D.A. Kyriakidis, D.P. Kessissoglou, *J. Inorg. Biochem.* 93 (2003) 256.
- [14] R.L. Kurtaran, T.A. Yildirim, D. Azaz, H. Namli, O. Atakol, *J. Inorg. Biochem.* 99 (2005) 1937.
- [15] R.D. Campo, J.J. Criado, E. Garcia, M.R. Hermosa, A. Jimenez-Sanchez, J.L. Manzano, E. Monte, E. Rodriguez-Fernandez, F. Sanz, *J. Inorg. Biochem.* 89 (2002) 74.
- [16] E.M. Jouad, G. Larcher, M. Allain, A. Riou, G.M. Bouet, M.A. Khan, X.D. Thanh, *J. Inorg. Biochem.* 86 (2001) 565.
- [17] W. Luo, X. Meng, X. Sun, F. Xiao, J. Shen, Y. Zhou, G. Cheng, Z. Ji, *Inorg. Chem. Commun.* 10 (2007) 1351.
- [18] Z. Afrasiabi, E. Sinn, W. Lin, Y. Ma, C. Campana, S. Padhye, *J. Inorg. Biochem.* 99 (2005) 1526.
- [19] M.C. Rodriguez-Arguelles, M. Belicchi Ferrari, F. Bisceglie, C. Pelizzi, G. Pelosi, S. Pinelli, M. Sassi, *J. Inorg. Biochem.* 88 (2004) 313.
- [20] S. Ramakrishnan, E. Suresh, A. Riyasdeen, M.A. Akbarsha, M. Palaniandavar, *Dalton Trans.* 40 (2011) 3245.
- [21] M. Frezza, S.S. Hindo, D. Tomco, M.M. Allard, Q.C. Cui, M.J. Heeg, D. Chen, Q.P. Dou, C.N. Verani, *Inorg. Chem.* 48 (2009) 5928.
- [22] S. Arounaguirri, D. Easwaramoorthy, A. Ashokkumar, A. Dattagupta, B.G. Maiyaa, *Proc. Indian Acad. Sci.* 112 (2000) 1.
- [23] N. Tang, J.G. Muller, C.J. Burrows, S.E. Rokita, *J. Inorg. Biochem.* 103 (2009) 210.
- [24] P.X. Xi, Z.H. Xu, F.J. Chen, Z. Zeng, X.W. Zhang, *Biochemistry* 38 (1999) 16648.
- [25] P. Krishnamoorthy, P. Sathyadevi, P. Thomas Muthiah, N. Dharmaraj, *RSC Adv.* 2 (2012) 12190.
- [26] E. Ramachandran, D. Senthil Raja, J.L. Mike, T.R. Wagner, M. Zeller, K. Natarajan, *RSC Adv.* 2 (2012) 8515.
- [27] H. Baruah, C.G. Barry, U. Bierbach, *Curr. Top. Med. Chem.* 4 (2004) 1537.
- [28] W.I. Sundquist, D.P. Bancroft, L. Chassot, S.J. Lippard, *J. Am. Chem. Soc.* 110 (1988) 8559.
- [29] J.R. Choudhury, M.W. Wright, C.S. Day, G. Saluta, G.L. Kucera, U. Bierbach, *J. Med. Chem.* 51 (2008) 7574.
- [30] C.W. Sun, H. Huang, M. Feng, X.L. Shi, X.D. Zhang, P. Zhou, *Bioorg. Med. Chem. Lett.* 16 (2006) 162.
- [31] Y.F. Yuan, J.T. Wang, M.C. Gimeno, A. Laguna, P.G. Jones, *Inorg. Chim. Acta* 324 (2001) 309.
- [32] C. Sacht, M.S. Datt, S. Otto, A. Roodt, *J. Chem. Soc., Dalton Trans.* (2000) 4579.
- [33] K.R. Koch, *Coord. Chem. Rev.* 216–217 (2001) 473.
- [34] M.M. Habtu, S.A. Bourne, K.R. Koch, R.C. Luckay, *New J. Chem.* 30 (2006) 1155.
- [35] H.G. Berhe, S.A. Bourne, M.W. Bredenkamp, C. Esterhuysen, M.M. Habtu, K.R. Koch, R.C. Luckay, *Inorg. Chem. Commun.* 9 (2006) 99.
- [36] C. Sacht, M.S. Datt, *Polyhedron* 19 (2000) 1347.
- [37] W. Hermindez, E. Spodine, L. Beyer, U. Schrtider, R. Richter, J. Ferreira, M. Pavani, *Bioinorg. Chem. Appl.* 3 (2005) 299.
- [38] W. Hermindez, E. Spodine, J.C. Munoz, L. Beyer, U. Schroder, J. Ferreira, M. Pavani, *Bioinorg. Chem. Appl.* 1 (2003) 271.
- [39] G. Binzet, N. Kulcu, U. Florke, H. Arslan, *J. Coord. Chem.* 62 (2009) 3454.
- [40] H. Arslan, U. Florke, N. Kulcu, M.F. Emen, *J. Coord. Chem.* 59 (2006) 223.
- [41] S. Pislewicz, J. Rust, C.W. Lehmann, F. Mohr, *Polyhedron* 29 (2010) 1968.
- [42] N. Selvakumaran, S.W. Ng, E.R.T. Tiekink, R. Karvembu, *Inorg. Chim. Acta* 376 (2011) 278.
- [43] N. Selvakumaran, A. Pratheepkumar, S.W. Ng, E.R.T. Tiekink, R. Karvembu, *Inorg. Chim. Acta* 404 (2013) 82.
- [44] APEX2 Program for Data Collection on Area Detectors BRUKER AXS Inc., 5465 East Cheryl Parkway, Madison, WI 53711–5373, USA.
- [45] SADABS, G.M. Sheldrick, Program for Absorption Correction of Area Detector Frames, BRUKER AXS Inc., 5465 East Cheryl Parkway, Madison, WI 53711–5373 USA.
- [46] G.M. Sheldrick, *Acta Crystallogr., Sect. A* 64 (2008) 112.
- [47] O.V. Dolomanov, L.J. Bourhis, R.J. Gildea, J.A.K. Howard, H. Puschmann, *J. Appl. Crystallogr.* 42 (2009) 339.
- [48] S. Satyanarayana, J.C. Dabrowiak, J.B. Chaires, *Biochemistry* 31 (1992) 9319.
- [49] J. Marmur, *J. Mol. Biol.* 3 (1961) 208.
- [50] M.Y. Song, Q. Wu, P.J. Yang, N.N. Luan, L.F. Wang, Y.M. Liu, *J. Inorg. Biochem.* 100 (2006) 1685.
- [51] L. Yang, D.R. Powell, R.P. Houser, *Dalton Trans.* (2007) 955.
- [52] A.M. Pyle, J.P. Rehmann, R. Meshoyrer, C.V. Kumar, N.J. Turro, J.K. Barton, *J. Am. Chem. Soc.* 111 (1989) 3051.
- [53] V. Rajendiran, R. Karthik, M. Palaniandavar, H.S. Evans, V.S. Periasamay, M.A. Akbarsha, B.S. Srinag, H. Krishnamurthy, *Inorg. Chem.* 46 (2007) 8208.
- [54] L.F. Tan, H. Chao, Y.F. Zhou, L.N. Ji, *Polyhedron* 26 (2007) 3029.
- [55] Q.L. Zhang, J.G. Liu, J.Z. Liu, H. Li, Y. Yang, H. Xu, H. Chao, L.N. Ji, *Inorg. Chim. Acta* 339 (2002) 34.
- [56] R. Kiełtyka, J. Fakhoury, N. Moitessier, H.F. Sleiman, *Chem. Eur. J.* 14 (2007) 1145.
- [57] S. Anbu, S. Kamalraj, B. Varghese, J. Muthumary, M. Kandaswamy, *Inorg. Chem.* 51 (2012) 5580.
- [58] R. Indumathy, S. Radhika, M. Kanthimathi, T. Weyhermuller, B.U. Nair, *J. Inorg. Biochem.* 101 (2007) 434.
- [59] M. Asadi, E. Safaei, B. Ranjbar, L. Hasani, *New J. Chem.* 28 (2004) 1227.
- [60] G.Y. Han, P. Yang, *J. Inorg. Biochem.* 91 (2002) 230.
- [61] H. Mansuri-Torshizi, R. Mital, T.S. Srivastava, H. Parekh, M.P. Chitnis, *J. Inorg. Biochem.* 44 (1991) 239.
- [62] R. Lakowicz, *Principles of Fluorescence Spectroscopy*, second ed., Plenum Press, New York, 1999.
- [63] D. Senthil Raja, N.S.P. Bhuvanesh, K. Natarajan, *Eur. J. Med. Chem.* 46 (2011) 4584.
- [64] P. Krishnamoorthy, P. Sathyadevi, A.H. Cowley, R.R. Butorac, N. Dharmaraj, *Eur. J. Med. Chem.* 46 (2011) 3376.
- [65] Z.Z. Chen, X.Z. Huang, Z.Z. Zheng, J.G. Xu, Z.B. Wang, *Analysis Method of Fluorescence*, third ed., Science Press, Beijing, 1990.
- [66] J.N. Miller, *Proc. Anal. Div. Chem. Soc.* 16 (1979) 203.
- [67] J.H. Tang, F. Luan, X.G. Chen, *Bioorg. Med. Chem.* 149 (2006) 3210.